The magnetic properties of single-domain particles with cubic anisotropy. II. Remanence curves

1993 J. Phys.: Condens. Matter 5 2793

(http://iopscience.iop.org/0953-8984/5/17/013)

J. Phys.: Condens. Matter 5 (1993) 2793–2808. Printed in the UK

The magnetic properties of single-domain particles with cubic anisotropy: II. Remanence curves

M Walker†, P I Mayo†, K O'Grady†, S W Charles†, R W Chantrell‡
† Magnetic Materials Research Group, School of Electronic Engineering Science, UCNW Bangor, Gwynedd, LL57 1UT, UK
‡ Department of Physics, Keele University, Keele, Staffordshire, ST5 5BG, UK

Received 4 December 1992, in final form 19 February 1993

Abstract. A comprehensive study of the remanence curve properties of an assembly of non-interacting single-domain particles with cubic magnetocrystalline anisotropy has been performed. The theoretical calculations presented represent an extension of the zero-temperature analysis of Joffe and Heuberger to include the effects of thermally activated magnetization reversal and particle size distribution. The numerical validity of these computations is completed through the analysis of interaction-sensitive Henkel plots, which confirm the non-interacting nature of the independently calculated remanence curves. The model system shows behaviour with intuition and analogous to similar models for the uniaxial case, with the exception of the expected increase in maximum remanence and decrease in energy barrier, i.e. remanence coercivity.

1. Introduction

In this paper we calculate remanence curves for systems of non-interacting single-domain particles with cubic magnetocrystalline anisotropy. Included in the model is a log-normal particle size distribution and the effects of thermal activation. The predictions made in this study are primarily based upon the theoretical and computational techniques described in the companion hysteresis loop model [1].

The measurement and interpretation of remanence curves as a means to characterize a wide variety of magnetic materials, especially those suitable for magnetic recording purposes, has received significant attention recently [2–4]. In particular, this attention has focused on the sensitivity of remanence curves to many-body interaction effects within particulate and thin-film recording media [5–7], and on the fundamental point that remanence measurements reflect only the irreversible changes in the magnetization, and as such examine the reversal process.

Theoretical predictions of remanence curves have been previously reported by a number of authors. Predictions of remanence curves for uniaxial fine particle systems have generally been based upon the methods of Stoner and Wohlfarth [8]. Gaunt [9] and Joffe [10] who extended the original Stoner–Wohlfarth theory to include the thermal dependence of the remanence coercivity for a uniaxial single-domain particle. Later Chantrell and co-workers [11, 12] calculated the isothermal remanent magnetization acquired from the demagnetized state of a more realistic system of fine particles with the magnetization easy axis aligned and randomly oriented with the applied field respectively. More recently, Walker and co-workers [13] have further extended this work by considering the effects of partial easy axis alignment with the applied field. These three final works have all incorporated the effects of thermally activated magnetization reversal and a log-normal distribution of particle sizes.

0953-8984/93/172793+16$07.50

Attempts at a similar treatment for multiaxial particle systems have been more limited. Joffe and Heuberger [14] have previously calculated the remanence of multiaxial systems at 0K. Consequently their calculations did not include the effects of thermally activated reversal, and were based upon a system of identical particle sizes. More recently, Geshev and co-workers [15, 16] have reported the results of an alternative approach to the prediction of hysteresis loops and remanence curves of multiaxial systems by considering the thermal variation of the saturation moment and anisotropy constants. However, this treatment does not take account of thermal activation of reversal.

2. The remanence curve model

Remanence curves are generally measured from either a demagnetized state, commonly known as an isothermal remanence curve (IRM), or from a previously saturated state, known as a DC demagnetization curve (DCD). The IRM curve, therefore, is a measure of the increase in remanence from an initially zero value to the positive saturation remanence, after the successive application and removal of increasingly positive DC fields. The analogous DCD curve is a measure of the reverse remanence from, say, the initially positive saturation remanence value to the negative saturation remanence, after the successive application and removal of increasingly negative applied fields.

2.1. The basic model

As previously discussed, the remanence is the magnetization remaining when the applied field is reduced to zero. Consequently it is necessary to compute the angle the magnetization vector relaxes into following the application and removal of an applied field. As with the preceding hysteresis loop paper [1], the angular coordinate systems adopted for these remanence curve calculations was first defined by Joffe and Heuberger [14] and is illustrated in figure 2 of [1]. Specifically, the orientation of any particle relative to the applied field $-H$ may be expressed in terms of the angles (θ, ψ). Similarly, the orientation of the magnetization vector relative to the principle anisotropy axes may be described in terms of the angles (γ, ϑ). The anisotropy constant is taken to be positive (i.e. $K > 0$) throughout this study.

The basic computational procedure for calculating the remanence of the system is as follows.

(1) The magnetic configuration of the model is initiated depending on the remanence curve studied.

(2) The particle orientation angle (θ, ψ) are both incremented from 0 to $\pi/2$ in steps of $\pi/90$ for each remanence curve field value.

(3) A steepest descent procedure is performed to obtain an approximate energy minimum for each field value. A Newton-Raphson method, for functions of two variables, is then used to obtain an accurate energy minimum and calculation of the magnetization angles (γ, ϑ).

(4) The applied field, h, is set to zero and the direction of the magnetization, I, is assumed to relax to the nearest easy axis, from which position the contribution to the remanence may be calculated (see sections 2.2.1 and 2.2.2).

2.1.1. Isothermal remanence. Considering the isothermal remanence (IRM) curve model first, the system is started from an initially demagnetized state in zero applied field. Thus, the only particles that contribute to the isothermal remanence are those whose magnetization

vector has traversed the energy barrier into the positive field direction and remain locked in their new positions when the field is removed.

Since only irreversible changes contribute to the remanence, if no transition has occurred the particle contribution to the remanence is represented by

$$\Delta \bar{I}_{r1} = 0. \tag{1}$$

After an irreversible change into the positive field direction, the particle contribution to the remanence is given by

$$\Delta \bar{I}_{r2} = \frac{1}{\pi} \sin 2\theta \qquad \text{for} \quad \gamma = 0, \vartheta = 0 \tag{2}$$

$$\Delta \bar{I}_{r3} = \frac{2}{\pi} \sin^2 \theta \cos \psi \qquad \text{for} \quad \gamma = \frac{\pi}{2}, \vartheta = 0 \tag{3}$$

$$\Delta \bar{I}_{r4} = \frac{2}{\pi} \sin^2 \theta \sin \psi \qquad \text{for} \quad \gamma = \frac{\pi}{2}, \vartheta = \frac{\pi}{2} \tag{4}$$

where the calculation of these remanence contributions is derived from the reduced magnetization formula in [1]:

$$\bar{I} = \frac{I}{I_s} = -\frac{2}{\pi} \int_0^{\frac{\pi}{2}} \int_0^{\frac{\pi}{2}} \left[\cos \gamma \cos \theta + \sin \gamma \sin \theta \cos (\psi - \varphi)\right] \sin \theta \, d\theta \, d\psi. \tag{5}$$

The magnetization vector orientation used during the calculation of the remanence at zero field corresponds to the principal anisotropy axes nearest to the (γ, ϑ) values obtained during the previous energy minimization routine, in the presence of the reduced applied field h. This is performed for all (θ, ψ) in the interval $\left(0, \frac{\pi}{2}\right)$, taking steps of $\pi/90$ in both angles. Thus, to predict IRM curves for a system of isolated single particles, the following integral must be performed:

$$\bar{I}_r = \int_0^{\frac{\pi}{2}} \int_0^{\frac{\pi}{2}} \Delta \bar{I}_m \, d\theta \, d\psi \tag{6}$$

where n runs from 1–4 for the complete integration, but has an integer value between 1–4 for an individual particle dependent upon the applied field relative to H_K and the particle's current condition of reversal, i.e. superparamagnetic, blocked following reversal to the applied field direction or blocked in the initial orientation direction. Additional information on this calculation is given in section 4 of [1].

2.1.2. DC demagnetization remanence. To obtain a DC demagnetization remanence curve the sample is first saturated in a large field (for the purposes of this study taken to be negative) and then removed to give a value for the saturation remanence ($I_r(\infty)$). A small positive DC field h is applied in the opposite direction to the saturating field and then removed to reveal the remanent state. As the reverse field h increases, the potential for the magnetization vectors to make an irreversible transition over the energy barrier increases.

In zero field, by extension of the hysteresis loop calculations in [1], the individual contribution that a particle makes to the remanence is given by

$$\Delta \bar{I}_d = -\frac{2}{\pi} \left[\cos \gamma \cos \theta + \sin \gamma \sin \theta \cos (\psi - \vartheta)\right] \sin \theta \, d\theta \, d\psi. \tag{7}$$

The possible remanent values of (γ, ϑ) in the negative saturating field direction are $(0,0), \left(\frac{\pi}{2}, 0\right), \left(\frac{\pi}{2}, \frac{\pi}{2}\right)$. Thus, if the energy barriers are sufficiently reduced to permit irreversible transitions, the magnetization vectors will move to new minima where the contributions to the remanence at those values of (γ, ϑ) are given by

$$\Delta \bar{I}_{d1} = -\frac{1}{\pi} \sin 2\theta \qquad \text{for} \quad \gamma = 0, \vartheta = 0 \tag{8}$$

$$\Delta \bar{I}_{d2} = -\frac{2}{\pi} \sin^2 \theta \cos \psi \qquad \text{for} \quad \gamma = \frac{\pi}{2}, \vartheta = 0 \tag{9}$$

$$\Delta \bar{I}_{d3} = -\frac{2}{\pi} \sin^2 \theta \sin \psi \qquad \text{for} \quad \gamma = \frac{\pi}{2}, \vartheta = \frac{\pi}{2}. \tag{10}$$

Clearly, if a magnetization vector subsequently resides in the positive reverse field direction the values of the possible remanence contributions are represented by

$$\Delta \bar{I}_{d4} = -\Delta \bar{I}_{d1} \tag{11}$$

$$\Delta \bar{I}_{d5} = -\Delta \bar{I}_{d2} \tag{12}$$

$$\Delta \bar{I}_{d6} = -\Delta \bar{I}_{d3}. \tag{13}$$

As with the associated IRM curve, the magnetization vector orientation used during the calculation of the remanence corresponds to the principal anisotropy axis nearest to the (γ, ϑ) values obtained in the presence of the reduced applied field h. The calculation is performed for all (θ, ψ) in the interval $\left(0, \frac{\pi}{2}\right)$, taking steps of $\pi/90$ in both angles. The total remanence is then obtained by a double integration over all the orientation configurations of (θ, ψ), such that

$$\bar{I}_d = \int_0^{\frac{\pi}{2}} \int_0^{\frac{\pi}{2}} \Delta \bar{I}_{dn} \, d\theta \, d\psi \tag{14}$$

where n runs from 1–6 for the complete integration over all particles, but has an integer value between 1–6 for a given particle.

2.2. The inclusion of thermal energy

The effects of thermal agitation on the remanence properties of both the IRM and DCD curves are obtained using the same criterion as for the previously reported hysteresis loop model, namely

$$T_{red} \geqslant \Delta\eta \tag{15}$$

where T_{red} is the reduced temperature and $\Delta\eta$ is the reduced energy barrier. Thus, if the thermal energy associated with a particle is greater than the energy barrier, a transition over the energy barrier takes place.

2.3. The inclusion of a particle size distribution

The effects of a particle size distribution have been investigated for both types of remanence curve by the inclusion of a volume fraction log-normal particle size distribution $f(y)$, given by

$$f(y)\,\mathrm{d}y = \frac{1}{\sigma(2\pi)^{1/2}\,y}\exp\left(\frac{-(\ln y)^2}{\sigma^2}\right)\mathrm{d}y \tag{16}$$

where $y(= D/D_v)$ is the reduced particle diameter and D_v the median particle diameter. The standard deviation of the distribution is represented by σ.

Clearly, the superparamagnetic particles will not contribute to the remanence since their magnetization vectors can relax to a random configuration in zero field. Thus, the equation describing the IRM curve for a fine-particle system with cubic anisotropy and log-normal particle size distribution, for $H < H_K$, is given by

$$\bar{I}_r = \int_0^{\frac{\pi}{2}}\int_0^{\frac{\pi}{2}} \Delta\bar{I}_m F_{b2}\,\mathrm{d}\theta\,\mathrm{d}\psi \tag{17}$$

where n has an integer value between 2–4 for an individual particle, corresponding to the appropriate anisotropy configuration. The term F_{b2} is related to the proportion of blocked particles that have made the transition into the positive field direction in reduced field, h, and is given by

$$F_{b2} = \int_{y_p(0)}^{y_p(h)} f(y)\,\mathrm{d}y. \tag{18}$$

If $H > H_K$, all the blocked particles will have been rotated into the field direction and the remanence is then described by

$$\bar{I}_r = \int_0^{\frac{\pi}{2}}\int_0^{\frac{\pi}{2}} \Delta I_m F_{b3}\,\mathrm{d}\theta\,\mathrm{d}\psi \tag{19}$$

where F_{b3} is given by

$$F_{b3} = \int_{y_p(0)}^{\infty} f(y)\,\mathrm{d}y. \tag{20}$$

Thus, (19) with (20) represents the saturation remanence for the system.

Similarly, the DC demagnetization remanence of the system for $H < H_K$ is given by

$$\bar{I}_d = \int_0^{\frac{\pi}{2}}\int_0^{\frac{\pi}{2}} \left(\Delta\bar{I}_{dn1}F_{b1} + \Delta\bar{I}_{dn2}F_{b2}\right)\mathrm{d}\theta\,\mathrm{d}\psi \tag{21}$$

where $n1 = 1$, 2 or 3 and $n2 = 4$, 5 or 6 for a given particle in (8)–(13) inclusively. The term F_{b2} is defined as in (18), and in a similar way F_{b1} is given by

$$F_{b1} = \int_{y_p(h)}^{\infty} f(y)\,\mathrm{d}y. \tag{22}$$

Thus, the $\Delta \bar{I}_{dn1}$ term of the integral in (21) corresponds to those particles that have not, as yet, reversed their magnetization vector to the direction of the reversing field, h. Likewise, the $\Delta \bar{I}_{dn2}$ term is associated with the particles that have reversed their magnetization.

As with the IRM curve, for reverse fields in excess of the anisotropy field, H_K, all the blocked particles will have reversed their magnetization direction, so that the saturation remanence is given by

$$\bar{I}_d = \int_0^{\frac{\pi}{2}} \int_0^{\frac{\pi}{2}} \Delta \bar{I}_{dn2} F_{b3} \, d\theta \, d\psi \tag{23}$$

where F_{b3} is given by (20).

Further details of the particle size distribution function, $f(y)$, and the associated calculations based on this distribution function, are given in the paper on our hysteresis loop calculations [1].

2.4. Switching field distribution

The differentials of the two primary remanence curves, termed χ_{irr}, give a measure of the switching field distribution in the material. The technique is commonly used to characterize recording media [17]. In the case of the model systems examined in this work the distribution arises due in part to the particle size distribution, since the value of the anisotropy constant is invariant for the given system. The orientation of the easy axes to the applied field direction will serve to increase the width of the distribution. In the work that follows the distributions have all been calculated from the IRM curves since data from the DCD curves would give the same result because there are no interactions in the system [18]. We have confirmed this result as a check on the self-consistency of our calculations.

3. Predictions of the single-particle volume model

3.1. Isothermal remanence curves

Figure 1 shows IRM curves for a monodispersed fine-particle system with cubic anisotropy and over a range of reduced temperatures, T_{red}.

At $T = 0$ K, the remanence is zero until the applied field $h = 0.274$, as only reversible changes can occur for $h < 0.274$. This prediction is as expected from our previous hysteresis loop study, which predicted that the first particle to make an irreversible rotation over the energy barrier has an orientation of ($\theta = 0°, \psi = 45°$) at the critical field of $h = 0.274$. Beyond $h = 0.274$ the remanence curve rises smoothly with field until it reaches its saturation remanence value when $h = 0.78$.

As with the hysteresis study, as the reduced temperature increases the increased thermal energy enables particles to overcome their energy barrier at lower applied fields. The reversible proportion of the curve decreases and the curves reach their saturation value in lower applied fields.

3.2. DC demagnetization remanence curves

Figure 2 illustrates the DC demagnetization curves for a fine-particle system with cubic anisotropy and identical particle size over a range of reduced temperatures, T_{red}. As T_{red} increases from zero, the value of the remanence coercivity, h_r, (where $\bar{I}_d(h_r) = 0$), decreases from its maximum value of 0.333 as the effects of increased thermal fluctuation become

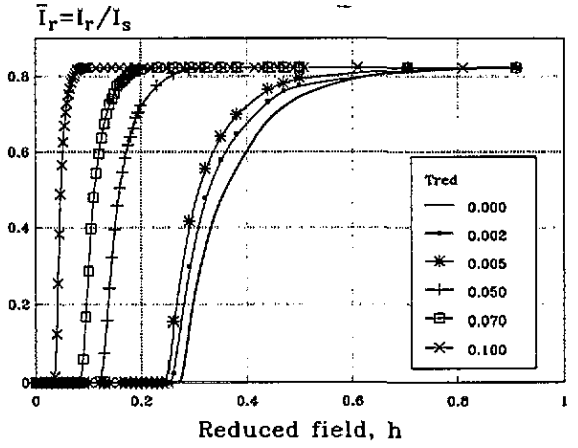

Figure 1. IRM curves for a system of monodispersed particles with cubic anisotropy.

significant. Figure 3 indicates the variation of the remanence coercivity, h_r, as a function of reduced temperature, T_{red}. At $T_{red} = 0.125$, h_r will be equal to zero due to the introduction of superparamagnetic behaviour.

In both the IRM curves of figure 1 and the DC demagnetization curves of figure 2 it is interesting to note that saturation remanence is attained prior to the application of the anisotropy field H_K. This effect is contrary to that predicted and experimentally observed in uniaxial systems, where fields of magnitude at least H_K are necessary for saturation. The reasons for this discrepancy lie in the complex energy surface associated with multiaxial particles. Thus, it is possible for magnetization reversal to take place with the magnetization vector following a path of least energy and traversing round a hard axis energy barrier, in lower applied fields than H_K, rather than crossing a hard axis directly.

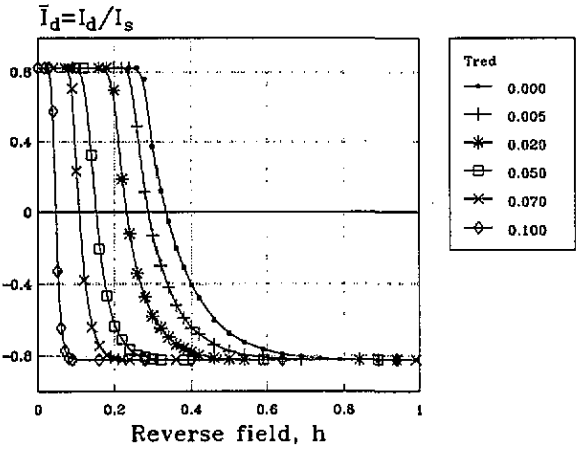

Figure 2. DCD curves for a system of monodispersed particles with cubic anisotropy.

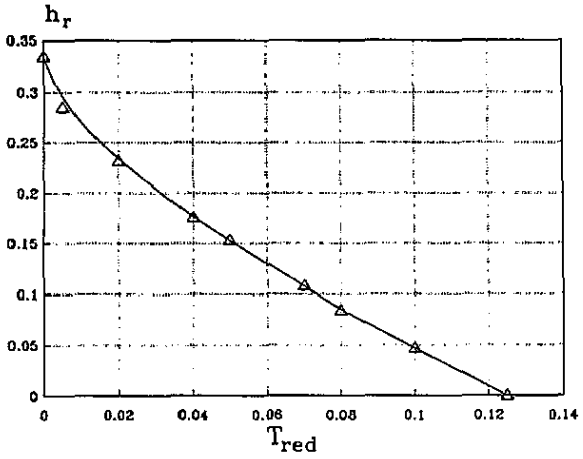

Figure 3. Effect of T_{red} on h_r for a system of monodispersed particles with cubic anisotropy.

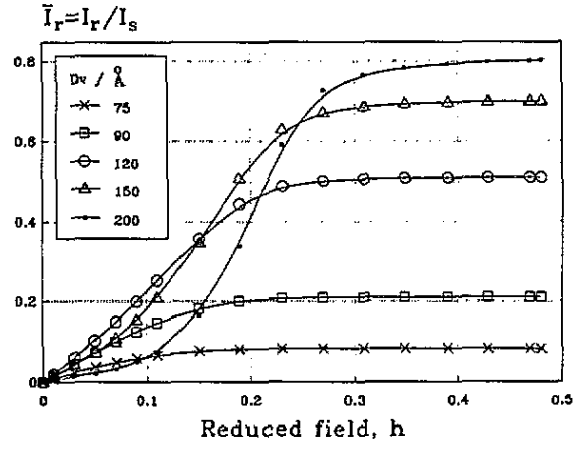

Figure 4. IRM curves for a system of particles at 100 K with $K = 2 \times 10^6$ erg cc^{-1}, $I_s = 400$ emu cc^{-1} and $\sigma = 0.3$.

4. Predictions for a system with a particle size distribution

4.1. Isothermal remanence curves

Figure 4 shows IRM curves for isolated particles, assuming a log-normal particle size distribution, as a function of variable median particle diameter, D_v. These predictions refer to a temperature of 100 K with $K = 2 \times 10^6$ erg cc^{-1}, $\sigma = 0.3$ and $I_s = 400$ emu cc^{-1}. As the median diameter is increased from 75 Å to 200 Å, the magnitude of the energy barrier also increases. Thus, larger applied fields are necessary to reduce the magnitude of the barriers so that magnetization reversal may occur. The increase in saturation remanence with increasing

median diameter is attributable to the reduction in the fraction of superparamagnetic particles present in the system.

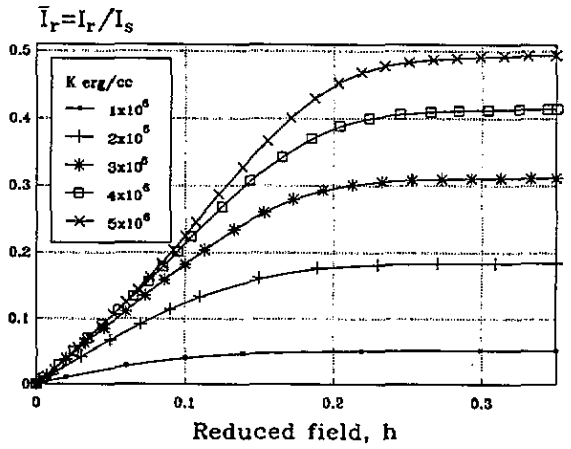

Figure 5. IRM curves for a system of particles at 150 K with $D_v = 100$ Å, $I_s = 400\,\text{emu cc}^{-1}$ and $\sigma = 0.3$.

Figure 5 indicates a similar set of IRM curves at 150 K, where the median diameter is held constant at 100 Å and the anisotropy constant K is increased from 1×10^6 to $5 \times 10^6\,\text{erg cc}^{-1}$. These remanence curves indicate a similar variation to that predicted as a function of increasing median diameter. However, as a consequence of increasing K, the anisotropy field H_K $(= 2K/I_s)$ is also increased, making the system more difficult to magnetize. Experimentally it is usually more desirable to maximize remanence by increasing the median diameter D_v and maintaining a small value of K, since it is generally easier experimentally to increase D_v rather than increase the value of K [19].

The dependence of IRM curves on temperature is shown in figure 6 ($D_v = 100$ Å, $K = 2 \times 10^6\,\text{erg cc}^{-1}$, $\sigma = 0.3$, $I_s = 400\,\text{emu cc}^{-1}$). Clearly, as the temperature is decreased the associated decrease in the thermal energy has the effect of raising the energy barrier, thus requiring higher applied fields to achieve magnetization reversal. The saturation remanence is also increased, as the temperature is reduced, due to the decrease in the fraction of superparamagnetic particles present in the system.

Figures 7 and 8 show a set of IRM curves and their associated switching field distributions (SFD) for a system at 40 K (with $K = 2.8 \times 10^6\,\text{erg cc}^{-1}$, $\sigma = 0.3$, $I_s = 400\,\text{emu cc}^{-1}$) and variable median diameter D_v. Clearly as the median diameter increases the remanence curve becomes sharper and the SFD curve becomes narrower as the particles reverse their magnetization over a smaller range of field values.

The data illustrate clearly an important effect of the finite temperature in relation to experimental observations. At 0 K the IRM curve has a discontinuity at the minimum field required to bring about irreversible rotation. Figure 1 shows that for a monodispersed system at a finite temperature the IRM curves retain an initial steep increase, albeit at a greatly reduced field; thermal agitation is not sufficient to produce a significant spread of switching fields for a given particle size. However, the introduction of thermal agitation does have the effect of introducing a dependence of the switching probability on the particle

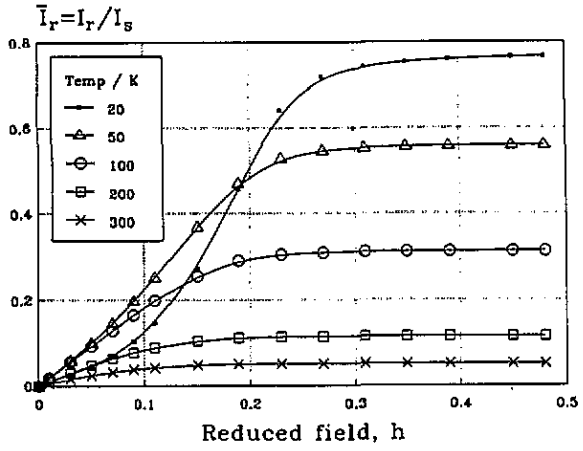

Figure 6. IRM curves for a system of cubic particles with $D_v = 100$ Å.

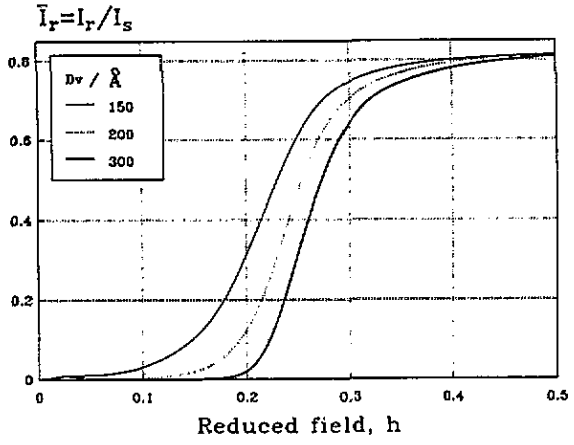

Figure 7. IRM curves for a system of multiaxial particles at 40 K with $K = 2.8 \times 10^6$ erg cc^{-1}, $\sigma = 0.3$ and $I_s = 400$ emu cc^{-1}.

size. Consequently, in a system with a particle size distribution the form of the IRM curve is drastically altered, as can be seen in figures 4–7, in that the curve increases smoothly from zero as a result of the distributed energy barrier. These data have a form that is more consistent with the experimental data, and similarity with the previously considered uniaxial case [12], and indicate the importance of calculations at a finite temperature for comparison with experimental data.

4.2. DC demagnetization remanence curves

Figure 9 illustrates a family of predicted DCD curves for a fine particle system at a temperature of 77 K with $K = 2 \times 10^6$ erg cc^{-1}, $\sigma = 0.3$ and $I_s = 400$ emu cc^{-1}. Both

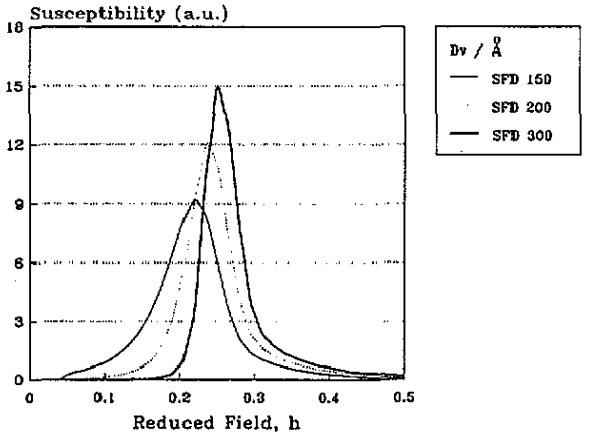

Figure 8. SFD for a system of multiaxial particles at 40 K with $K = 2.8 \times 10^6$ erg cc^{-1}, $\sigma = 0.3$ and $I_s = 400$ emu cc^{-1}.

the saturation remanence and the remanent coercivity, h_r, are observed to increase as D_v increases from 90 Å to 200 Å. This is expected, since an increase in D_v will reduce the fraction of superparamagnetic particles present in the sample and increase the magnitude of the energy barrier. For the curve with $D_v = 200$ Å, the saturation remanence and remanence coercivity values are close to the maximum values obtained at 0 K (0.823 and 0.333 respectively), indicating that most of the particles in the assembly are blocked at this value of median particle diameter.

A similar set of DCD remanence curves at 100 K are indicated in figure 10, where the median diameter is held constant at $D_v = 90$ Å and the anisotropy constant, K, is varied between 2×10^6 and 6×10^6 erg cc^{-1}. Even at the largest value of anisotropy constant, $K = 6 \times 10^6$ erg cc^{-1}, the saturation remanence does not attain the maximum possible value of 0.823 because of the significant contribution of the superparamagnetic particles present in the system.

Figure 11 illustrates the variation of h_r with temperature for a system with cubic anisotropy, where $D_v = 100$ Å, $K = 2 \times 10^6$ erg cc^{-1}, $\sigma = 0.3$ and $I_s = 400$ emu cc^{-1}. The more general case of this variation, independent of median particle diameter D_v, is shown in the insert of figure 11 as a function of the temperature-related ratio D_p/D_v, again for a system where $\sigma = 0.3$.

4.3. Interaction curves

Much recent work into the measurement and characterization of interactions in magnetic systems using remanence curves has been based upon the examination of the Wohlfarth relation [18]

$$I_d(H) = I_r(\infty) - 2I_r(H). \tag{24}$$

This equation relates the two principal remanence curves in the absence of interparticle interactions. Henkel [20] first used this relationship to examine interactions by plotting the DC demagnetization remanence (I_d) as a function of the isothermal remanence (I_r).

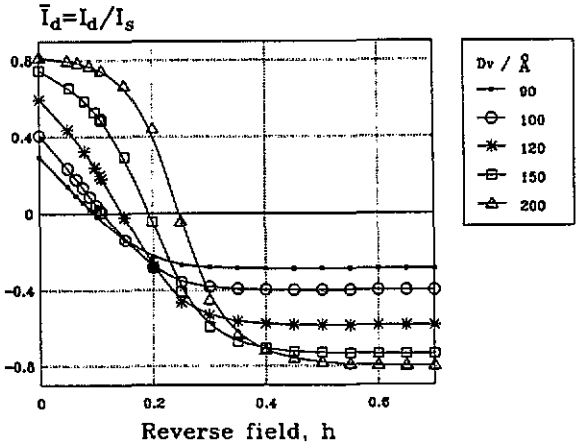

Figure 9. DCD curves for a system at 77 K with $K = 2 \times 10^6$ erg cc^{-1} and $\sigma = 0.3$.

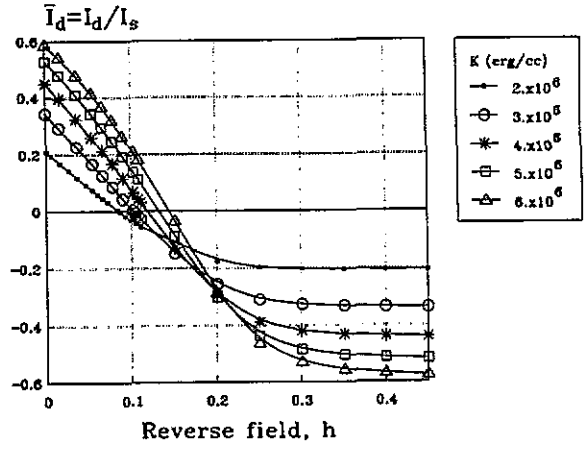

Figure 10. DCD curves for a system at 100 K with $D_v = 90$ Å and $\sigma = 0.3$.

Thus, in the absence of interactions, a linear relationship should be obtained. Moreover, this technique can also be used as a valuable tool to confirm the self-consistency of the numerical computations and the accuracy of the energy minimization algorithm used in our computations.

Figure 12 shows a set of isothermal and DC demagnetization remanence curves for a system with a mean particle diameter of 110 Å and $\sigma = 0.3$, $K = 2 \times 10^6$ erg cc^{-1} over a range of temperatures. As expected, the shape of the remanence curves changes with temperature and the maximum value of saturation remanence decreases with increasing temperature.

Figure 13 is the associated Henkel plots (I_d against I_r) for the data sets in figure 12. The

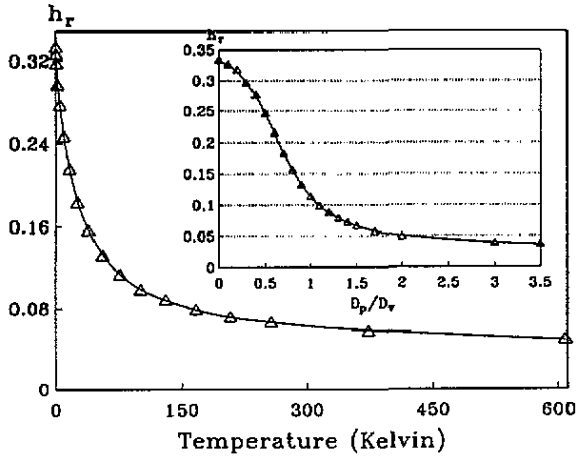

Figure 11. Effect of temperature on h_r for a system with cubic anisotropy, where $D_v = 100$ Å, $K = 2 \times 10^6$ erg cc^{-1} $\sigma = 0.3$ and $I_s = 400$ emu cc^{-1}. Inset: the effect of D_p/D_v on h_r for a system with cubic anisotropy.

linearity displayed by the four data sets in figure 13 indicates that the Wohlfarth relationship denoted in (24) is validated. It is usual to display Henkel plots of the remanence curve data normalized with respect to the maximum saturation remanence. However, on this occasion, to enable the variations in the maximum saturation remanence to be observed this Henkel plot data is displayed in terms of the absolute reduced remanence.

In principle it would not necessarily be expected that the Henkel plot for cubic systems would be linear, since the initial magnetization configuration is different in each case, i.e. a random distribution for the IRM case and all the moments lying in the nearest easy axis direction to the field direction for the DCD case. However, it must be realized that the cubic anisotropy gives rise to a complex energy surface, unlike the uniaxial case where all reversals must traverse a hard direction. Thus by moving across the energy surface avoiding hard axes, the energy barrier distribution in both the IRM and DCD cases is the same. Hence a linear Henkel plot is expected in the absence of interactions.

Figure 13 is therefore a significant result, which justifies the validity of the whole computational approach of this study and, in particular, the accuracy of the numerical energy minimization algorithms used. This result, however, is in marked contrast to the recent work of Geshev *et al* [16] on multiaxial fine-particle systems, where non-linear Henkel plots were obtained. At present we cannot account for this discrepancy.

4.4. The temperature decay of remanence

Temperature decay of remanence curves represent the variation of saturation remanence with temperature and are often used to experimentally determine the magnitude of the anisotropy constant K [21]. Figure 14 shows the predicted decay of remanence curves for a multiaxial material with cubic anisotropy for a range of median particle diameters, D_v, where $K = 2 \times 10^6$ erg cc^{-1}, $\sigma = 0.3$ and $I_s = 400$ emu cc^{-1}.

As expected, maximum remanence is achieved at 0 K when all the particles in the system are blocked. As the temperature increases, the fraction of superparamagnetic particles present increases and the remanence decays logarithmically with temperature. This data is

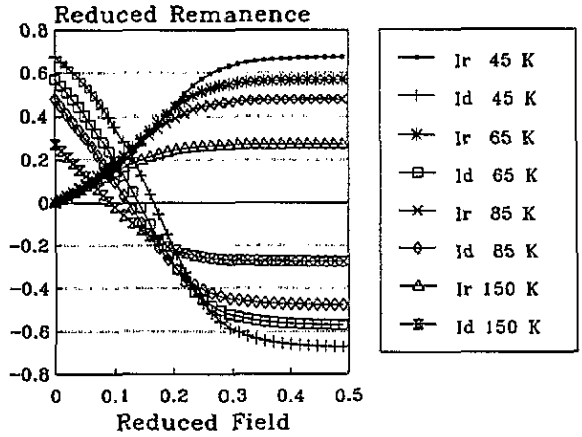

Figure 12. Pairs of principal remanence curves as a function of temperature, $D_v = 110$ Å, $K = 2 \times 10^6$ erg cc^{-1}, $\sigma = 0.3$, $I_s = 400$ emu cc^{-1}.

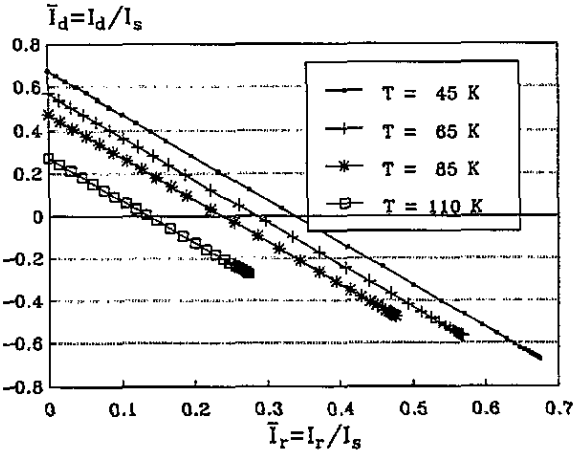

Figure 13. Henkel plots for remanence curve data displayed in the previous figure.

similar in form to the experimental observations for uniaxial systems [21]. At the present time we are not aware of any data of this type for systems with cubic anisotropy that would enable an accurate measure of the anisotropy constant K. When the remanence has decayed to half its value at 0 K, half of the magnetic volume has relaxed. The temperature at which this occurs is called the mean blocking temperature, T_K. Since the median diameter is known, a value of the effective anisotropy constant, where $K > 0$, can be estimated from the relation

$$K = \frac{600kT_K}{\pi D_v^3}. \tag{25}$$

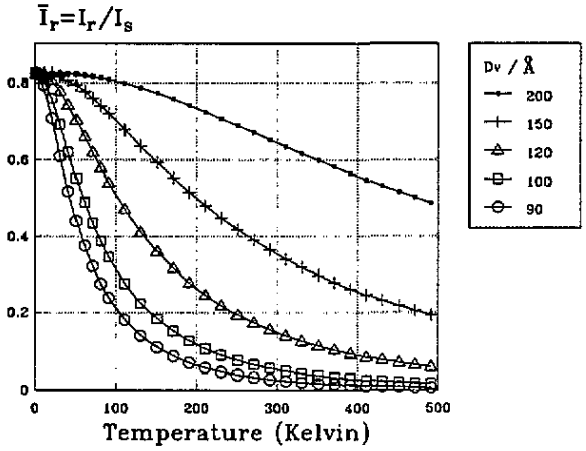

Figure 14. Decay of remanence curves for a system with $K = 2 \times 10^6 \,\mathrm{erg\,cc^{-1}}$, $\sigma = 0.3$ and $I_s = 400 \,\mathrm{emu\,cc^{-1}}$.

5. Conclusions

In this paper we have used a numerical model to predict the two principal magnetizing and demagnetizing remanence curves for non-interacting single-domain fine-particle systems with cubic anisotropy. The effects of temperature, particle size and particle size distribution have been extensively examined. The self-consistency of our predictions has been confirmed through a comparison of pairs of independently obtained remanence curves and an examination of Henkel plots.

References

[1] Walker M, Mayo P I, O'Grady K, Charles S W and Chantrell R W 1993 *J. Phys.: Condens. Matter* **5** 2779
[2] Pinkerton F E 1986 *IEEE Trans. Magn.* **22** 922
[3] Gaunt P, Hadjipanayis G and Ng C 1986 *J. Magn. Magn. Mater.* **54–57** 841
[4] Spratt G W D, Bissell P R, Chantrell R W and Wohlfarth E P 1988 *J. Magn. Magn. Mater.* **75** 309
[5] Corradi A R and Wohlfarth E P 1978 *IEEE Trans. Magn.* **14** 861
[6] Mayo P I, Bradbury A, Chantrell R W, Kelly P E, Jones H E and Bissell P R 1990 *IEEE Trans. Magn.* **26** 228
[7] Kelly P E, O'Grady K, Mayo P I and Chantrell R W 1989 *IEEE Trans. Magn.* **21** 3881
[8] Stoner E C and Wohlfarth E P 1948 *Phil. Trans. R. Soc.* A **240** 664
[9] Gaunt P 1968 *Phil. Mag.* **17** 263
[10] Joffe I 1969 *J. Phys. C: Solid State Phys.* **2** 1537
[11] Chantrell R W, O'Grady K, Bradbury A, Charles S W and Popplewell J 1985 *J. Phys. D: Appl. Phys.* **18** 2505
[12] Chantrell R W, O'Grady K, Bradbury A, Charles S W and Hopkins N 1987 *IEEE Trans. Magn.* **23** 204
[13] Walker M, Chantrell R W, O'Grady K and Charles S W 1988 *J. Physique* **49** C8-1819
[14] Joffe I and Heuberger R 1974 *Phil. Mag.* **29** 1051
[15] Geshev J, Popov O, Masheva V and Mikhov M 1990 *J. Magn. Magn. Mater.* **92** 185
[16] Geshev J and Mikhov M 1992 *J. Magn. Magn. Mater.* **104–107** 1569
[17] O'Grady K 1990 *IEEE Trans. Magn.* **26** 1870

[18] Wohlfarth E P 1958 *J. Appl. Phys.* **29** 595
[19] Chantrell R W and O'Grady K 1992 *J. Phys. D: Appl. Phys.* **25** 1
[20] Henkel O 1964 *Phys. Status Solidi* **7** 919
[21] Chantrell R W, El-Hilo M and O'Grady K 1991 *IEEE Trans. Magn.* **27** 3570